The 8th European Congress on Computational Methods in Applied Sciences and Engineering
ECCOMAS Congress 2022
5 – 9 June 2022, Oslo, Norway

EFFECT OF HYDROGEN ADDITION TO METHANE-AIR JET FLAME BASED ON SANDIA FLAME D

J. LIU[1], C. D. PÉREZ-SEGARRA[1], J. RIGOLA[1] AND F. X. TRIAS[1]

[1]Heat and Mass Transfer Technological Center, Technical University of Catalonia
Carrer de Colom 11, 08222 Terrassa (Barcelona), Spain; www.cttc.upc.edu
{jiannan.liu, cdavid.perez.segarra, joaquim.rigola, francesc.xavier.trias}@upc.edu

Key words: Sandia flame D, Hydrogen addition, Chemical mechanisms, Open FOAM.

Abstract. The present study investigates the effect of hydrogen addition to methane-air jet flame based on Sandia flame D. For this purpose, RANS simulations with a global four-step mechanism were first compared with other reduced (1-step, 2-step) and detailed mechanisms (DRM-19, GRI-Mech 3.0) using the standard $k-\varepsilon$ model. The accuracy of the simulations was further verified based on the LES wall-adapting local eddy-viscosity (WALE) model. The turbulence-chemistry interaction was described by the eddy dissipation concept (EDC) model. All simulations were carried out with Open FOAM. Simulation results with two main turbulence models, RANS and LES, were compared with available experimental data. The results showed the good agreement between experimental data and simulations for the selected flame using the global four-step mechanism. Other reduced and detailed chemical mechanisms were not attractive because the accuracy and computational cost were insufficient. CH_4-H_2 blending jet flame (5% CH_4+20% H_2) based on flame D geometry was simulated to verify that RANS and LES can have similar and reasonable results. After that, the influence of different mixture proportions was analyzed using the RANS model and the global four-step mechanism. It was observed that the addition of hydrogen accelerates the propagation and attenuation of jet flame under conditions of the same geometry and constant Re number. But it allowed the flame to maintain the same peak temperature while reducing carbon dioxide emission and oxygen consumption.

1 INTRODUCTION

Hydrogen fuel is increasingly being seen as clean energy in the future. Unlike the carbon products from fossil fuels like natural gas, hydrogen combustion with oxygen will produce only water, effectively avoiding environmental pollution and has excellent combustion performance. In industrial production, one effective utilization method is delivering hydrogen with natural gas along with the pipe system for combustion requests. Hence, hydrogen enrichment of fuels like methane is an attractive research field[1,2].

The fundamental combustion characteristics of CH_4-H_2 flame are necessary to understand. A study of the ignition delay time of the homogeneous hydrogen-methane-air mixture at high pressure was reported by Huang[3]. It was found that the generation and consumption of H radicals play a significant role in the effect of ignition delay time. Huang[4] observed by experiment that the combustion of hydrogen-methane mixture fuel could have lower emission

and higher thermal efficiency. Fordoei[5] also found that adding hydrogen to methane significantly decreases the ignition delay time and was effective in maintaining flame characteristics in the conversion of the combustion system from air fuel to oxygen-enriched fuel. On the other hand, turbulent non-premixed jet flame with CH_4-H_2 blending fuel is an attracting flame. Karbasi[6] focused on both experimental and numerical studies of the flame stability when adding hydrogen to methane diffusion flame. The higher stability can be achieved by the addition of hydrogen on both fuel jet and co-flow jet. The turbulence chemistry interaction in turbulent hydrogen-enriched methane jet flame had been studied with LES by Deniz[7]. Amir[8] considered three different hydrogen methane fuel mixtures on turbulent non-premixed jet flame with detailed chemical mechanisms like DRM-22 and GRI-Mech 2.11. It was reported that the addition of hydrogen to methane led to high levels of OH, HCO, and CH2O, which were beneficial for higher heat release and reaction intensity.

The present study aims to better understand the effect of hydrogen addition to methane-air jet flame. The Sandia flame D[9] is selected to predict the methane-air jet flame characteristics. For this purpose, the flame D will be simulated with different chemical kinetic mechanisms by RANS, including the 1-step[10], 2-step[11], 4-step[12], DRM-19[13], and GRI-Mech 3.0[14] mechanisms. Simulation results are compared with experimental data. The results with the 4-step mechanism are reasonably good considering the accuracy and computational cost. LES modelling of the flame D with the WALE model using the 4-step mechanism is then simulated to compare with RANS' results and experimental data, further validating the accuracy of the 4-step mechanism. LES modelling of mixture CH_4-H_2 (5%CH_4+20%H_2) fuel jet flame based on flame D (same conditions except for fuel) is simulated to compare with RANS's results. Based on the previous analysis, RANS is selected to study the CH_4-H_2 mixtures fuel jet flame at various compositions (from 25%CH_4+0%H_2 to 0%CH_4+25%H_2). Barlow and Carter[15]'s pure hydrogen jet flame experiment is used for predicting the pure non-premixed hydrogen jet flame in simulations.

2 MATHEMATICAL MODELLING

2.1 Governing equations

The governing equations are the multi-species compressible reacting flow Navier-Stokes equations.

The continuity equation

$$\frac{\partial \rho}{\partial t} + \frac{\partial \rho u_i}{\partial x_i} = 0 \tag{1}$$

where ρ is the density, t is the time, u_i is the velocity component in i-th direction.

The momentum equation

$$\frac{\partial \rho u_j}{\partial t} + \frac{\partial \rho u_i u_j}{\partial x_i} = -\frac{\partial p}{\partial x_j} + \frac{\partial \tau_{ij}}{\partial x_i} + \rho \sum_{k=1}^{N} Y_k f_{k,j} \tag{2}$$

where p is the pressure, τ_{ij} is the viscous stress tensor, Y_k is the mass fraction of k-th specie, and $f_{k,j}$ is the volume force acting on k-th specie in j-th direction. The viscous stress tensor can be expressed as

$$\tau_{ij} = \mu\left(\frac{\partial u_i}{\partial u_j} + \frac{\partial u_j}{\partial x_i}\right) - \frac{2}{3}\mu\frac{\partial u_k}{\partial x_k}\delta_{ij} \tag{3}$$

where μ is the dynamic viscosity calculated by Sutherland model, and δ_{ij} is the Kronecker symbol.

The energy equation

$$\frac{\partial \rho h_s}{\partial t} + \frac{\partial \rho u_i h_s}{\partial x_i} + \frac{\partial \rho K}{\partial t} + \frac{\partial \rho u_i K}{\partial x_i} = -\frac{\partial q_i}{\partial x_i} + \frac{\partial p}{\partial t} + \frac{\partial \tau_{ij} u_i}{\partial x_j} + \dot{Q} + \dot{\omega}_T + \rho\sum_{k=1}^{N} Y_k f_{k,i} V_{k,i} \tag{4}$$

where h_s is the sensible enthalpy, K is the fluid kinetic energy, q_i is the heat flux, $\dot{\omega}_T$ is the heat release due to combustion, and $V_{k,i}$ is the i-th component of the diffusion velocity V_k of k-th specie. In the present work, the volume force term f_k, the heat source term $\dot{Q}$, and the work carried out by the viscous stress term $\frac{\partial(\tau_{ij}u_i)}{\partial x_j}$ are neglected, which is similar to the work by Mousavi[16].

The species transport equation

$$\frac{\partial \rho Y_k}{\partial t} + \frac{\partial}{\partial x_i}\left(\rho\left(u_i + V_{k,i}\right)Y_k\right) = \dot{\omega}_k \tag{5}$$

where $\dot{\omega}_k$ is the reaction rate of k-th specie; the diffusion term can be assumed as

$$V_{k,i}Y_k = -D_k\frac{\partial Y_k}{\partial x_i} \tag{6}$$

where D_k is the diffusion coefficient of k-th specie.

2.2 Turbulence models

2.2.1 Reynolds-average simulation model

The standard $k-\varepsilon$ model is the most commonly used turbulence model on RANS simulation, proposed by Jones and Launder[17]. The flow is assumed as a fully turbulent flow. Two additional transport equations are introduced to predict the properties of a turbulent flow without prior knowledge of flow structure. The turbulent kinetic energy $\tilde{k}$ and the dissipation rate $\tilde{\varepsilon}$ are described by their transport equations,

$$\frac{\partial \bar{\rho}\tilde{k}}{\partial t} + \frac{\partial \bar{\rho}\tilde{u}_i\tilde{k}}{\partial x_i} = \frac{\partial}{\partial x_i}\left(\left(\mu + \frac{\mu_t}{\sigma_k}\right)\frac{\partial \tilde{k}}{\partial x_i}\right) + P_k - \bar{\rho}\tilde{\varepsilon} \tag{7}$$

$$\frac{\partial \bar{\rho}\tilde{\varepsilon}}{\partial t} + \frac{\partial \bar{\rho}\tilde{u}_i\tilde{\varepsilon}}{\partial x_i} = \frac{\partial}{\partial x_i}\left(\left(\mu + \frac{\mu_t}{\sigma_\varepsilon}\right)\frac{\partial \tilde{\varepsilon}}{\partial x_i}\right) + C_{\varepsilon 1}\frac{\tilde{\varepsilon}}{\tilde{k}}P_k - C_{\varepsilon 2}\bar{\rho}\frac{\tilde{\varepsilon}^2}{\tilde{k}} \tag{8}$$

where P_k is the source term calculated as

$$P_k = \bar{\rho}\widetilde{u_i''u_j''}\frac{\partial \tilde{u}_i}{\partial x_i} \tag{9}$$

The turbulent viscosity μ_t is expressed as

$$\mu_t = \bar{\rho}\nu_t = \bar{\rho}C_\mu\frac{\tilde{\varepsilon}^2}{\tilde{k}} \tag{10}$$

where the model constants are

$$C_\mu = 0.09;\ \sigma_k = 1.0;\ \sigma_\varepsilon = 1.3;\ C_{\varepsilon 1} = 1.44;\ C_{\varepsilon 2} = 1.92$$

2.2.2 Large-eddy simulation model

The Wall-Adapting Local Eddy-viscosity model (WALE) is an algebraic eddy viscosity model, which is proposed by Nicoud[18]. It is based on the square of the velocity gradient tensor, considering both the strain rate and rotation rate of the turbulent structure. The sub-grid scale eddy viscosity ν_{sgs} is expressed as

$$\nu_{sgs} = (C_w \Delta)^2 \frac{\left(S_{ij}^d S_{ij}^d\right)^{\frac{3}{2}}}{\left(\bar{S}_{ij}\bar{S}_{ij}\right)^{\frac{5}{2}} + \left(S_{ij}^d S_{ij}^d\right)^{\frac{5}{4}}} \tag{11}$$

where C_w is the model constant, S_{ij}^d is the traceless symmetric part of the square of the velocity gradient tensor, and $\bar{S}_{ij}$ is the resolved scale strain rate tensor.

$$\bar{S}_{ij} = \frac{1}{2}\left(\frac{\partial \tilde{u}_i}{\partial x_j} + \frac{\partial \tilde{u}_j}{\partial x_i}\right)$$
$$S_{ij}^d = \frac{1}{2}\left(\tilde{g}_{ij}^2 + \tilde{g}_{ji}^2\right) - \frac{1}{3}\delta_{ij}\tilde{g}_{kk}^2 \tag{12}$$

where $\tilde{g}_{ij} = \frac{\partial \tilde{u}_i}{\partial x_j}$ is the velocity gradient tensor, and δ_{ij} is the Kronecker symbol.

2.3 Combustion model

The Eddy Dissipation Concept (EDC) model is based on the energy cascade assumption proposed by Magnussen and Ertesvag[19]. It is assumed that the turbulent mixing and chemical reactions occur in only fine structures. Based on the assumption of isotropic turbulence, introducing the turbulent kinetic energy and its dissipation rate, the mass fraction occupied by the fine structure can be expressed as

$$\Upsilon^* = 4.6\left(\frac{\nu\tilde{\varepsilon}}{\tilde{k}}\right)^{\frac{1}{2}} \tag{13}$$

The filtered reaction rate $\widetilde{\dot{\omega}}_k$ is calculated as

$$\widetilde{\dot{\omega}}_k = -\frac{\bar{\rho}\dot{m}\chi}{1 - \Upsilon^*\chi}\left(\tilde{Y}_s - \tilde{Y}_s^*\right) \tag{14}$$

where $\tilde{Y}_s$ and $\tilde{Y}_s^*$ are the mean mass fraction and the fine structure mass fraction of s-th specie. $\dot{m} = 11.2\,\tilde{\varepsilon}/\tilde{k}$ is the mass transfer between the fine structures and surrounding fluids. χ is the reacting fraction of the fine structures where the calculation is detailed in Magnussen and Ertesvag.

3 PROBLEM SETUP

The Sandia flame D is a non-premixed methane-air jet flame experimentally tested by Sandia National Laboratory. There are three types of pre-inlets, including the main jet, pilot jet, and co-flow jet. The main jet contains 25% by volume of CH_4 and 75% air, corresponding to an equivalence ratio of 3.174. The pilot jet is a mixture of C_2H_2, H_2, CO_2, N_2, and air. The co-flow jet consists of air. The bulk velocity of the main jet, pilot jet, and co-flow jet are 49.6m/s, 11.4m/s, and 0.9m/s, respectively. The Reynolds number of the main jet mixture is 22400. The inner diameter of the main jet is 7.2mm, while the inner and outer annulus diameter of the pilot jet is 7.7mm and 18.2mm, respectively. The outer annulus diameter of the co-flow jet is 150mm,

and the length of the downstream domain is 500mm.

Figure 3.1 shows the basic sketch of the Sandia flame D computational geometry. Tables 3.1 and 3.2 describe the inlet conditions of the mass fraction of species on the pre-inlet patches and boundary conditions on the patches.

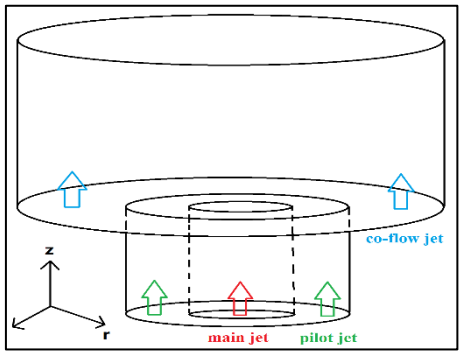

Figure 3.1: Sketch of the Sandia flame D geometry

Table 3.1: Initial conditions of species on pre-inlet patches

	CH_4	O_2	H_2O	CO_2	N_2
Main jet	0.1561	0.1966	0	0	0.6473
Pilot jet	0	0.054	0.0942	0.1098	0.742
Co-flow jet	0	0.23	0	0	0.77

Table 3.2: boundary conditions on patches

	pressure [Pa]	T [K]	U [m/s]	Y_i
Main jet	$\frac{\partial p}{\partial z} = 0$	$T_{fix} = 294$	U_{fix}= (0, 0, 49.6)	Table 3.1
Pilot jet	$\frac{\partial p}{\partial z} = 0$	$T_{fix} = 1880$	U_{fix}= (0, 0, 11.4)	
Co-flow jet	$\frac{\partial p}{\partial z} = 0$	$T_{fix} = 291$	U_{fix}= (0, 0, 0.9)	
wallTube	$\frac{\partial p}{\partial r} = 0$	$\frac{\partial T}{\partial r} = 0$	$U_{fix} = 0$	$\frac{\partial Y_i}{\partial r} = 0$
wallOutside	$\frac{\partial p}{\partial r} = 0$	$\frac{\partial T}{\partial r} = 0$	$U_{fix} = 0$	$\frac{\partial Y_i}{\partial r} = 0$
outlet	$p_{fix} = 1e5$	$\frac{\partial T}{\partial z} = 0$	$\frac{\partial U}{\partial z} = 0$	$\frac{\partial Y_i}{\partial z} = 0$

4 RESULTS AND DISCUSSIONS

The presented flame simulations are conducted using reactingFom solver of Open FOAM. The RANS simulations of Sandia flame D are presented with reduced and detailed chemical kinetic mechanisms. Subsequently, the 4-step mechanism is further validated on LES simulation with WALE model. Based on the pre-conditions of the same geometry and constant Reynolds number as flame D, the inlet velocity of the main jet is revised according to the corresponding CH_4-H_2 blending proportions. The effect of hydrogen addition on methane fuel jet flame is studied by a series of fuel blending proportions of CH_4-H_2, from 25%CH_4-0%H_2 to

0%CH_4-25%H_2. The pure 25%H_2 jet flame is simulated with three different chemical mechanisms, and simulation results of H_2-air jet flame by Barlow and Carter[15] are compared to their experimental data for validation.

4.1 RANS simulations of Sandia flame D

Figure 4.1 displays the RANS results of mean mass fraction of CH_4, temperature, and velocity along the center line of flame with reduced and detailed chemical mechanisms compared to the experimental data. The predicted results with 4-step, DRM19, and GRI-Mech 3.0 show better agreement with experimental data than those with 1-step and 2-step mechanisms. However, it is found that the calculation time of cases with detailed mechanisms is at least seven times higher than cases with reduced mechanisms. Based on the considerations of accuracy and computational cost, the 4-step mechanism is regarded as a reasonable selection.

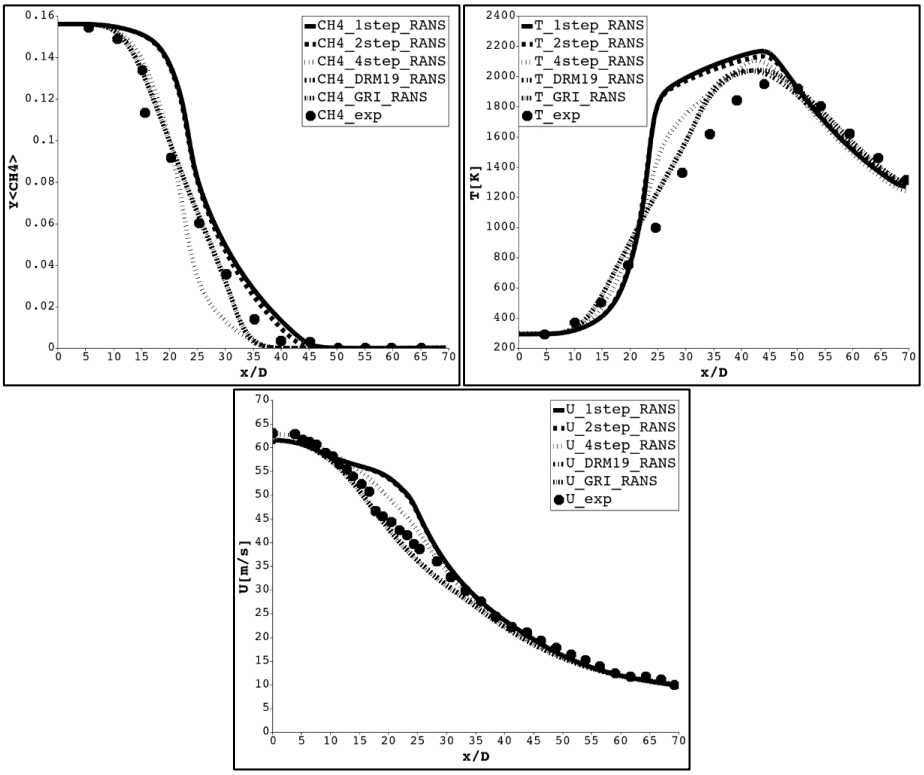

Figure 4.1: Mean CH_4, temperature, and velocity along the centerline of Sandia flame D on RANS cases; experimental data from [9]

4.2 LES simulations of Sandia flame D

The results of the mean mass fraction of CH_4, temperature, and velocity along the centerline of flame with the WALE turbulence model and the 4-step mechanism are shown in figure 4.2. It is apparent that predicted results are in reasonable agreement with the measured data. It is further validated that 4-step mechanism is an appropriate chemical mechanism for this jet flame simulation.

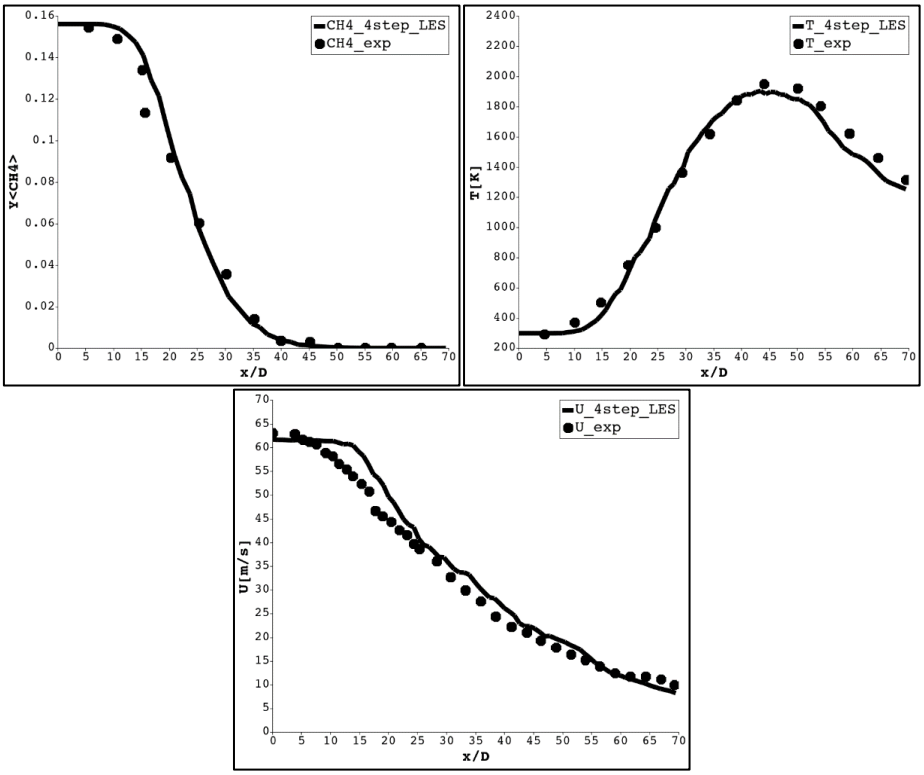

Figure 4.2: Mean CH_4, temperature, and velocity along the centerline of Sandia flame D on LES case; experimental data from [9]

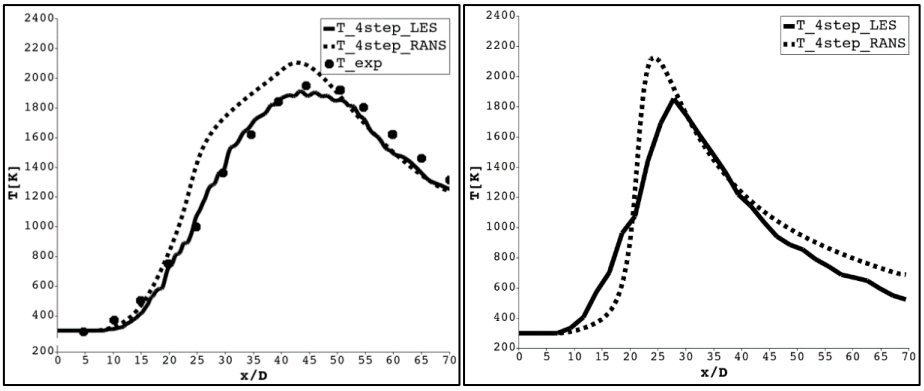

Figure 4.3: Mean temperature along the centerline of Sandia flame D (left); experimental data from [9] ; mean temperature along the centerline of 5%CH_4+20%H_2 blending jet flame (right)

4.3 RANS and LES simulations of 5%CH_4+20%H_2 blending jet flame

Figure 4.3 describes the mean temperature along the centerline of flame between RANS and LES on flame D (pure CH_4) and 5%CH_4+20%H_2 blending fuel jet flame. Figure 4.4 shows the mean mass fraction of CH_4, and velocity between RANS and LES on the same blending fuel jet flame. It costs 10 minutes for RANS case with 4 cores to run the 0.1s simulation time. However, it takes 180 hours for LES case using 160 cores to reach the 0.15s simulation time. Hence, although there are some discrepancies between these two approaches, it is still

acceptable to use RANS model on the blending fuel jet flame simulations because it can obtain accurate enough results as LES case but the cost of computational resource is much lower.

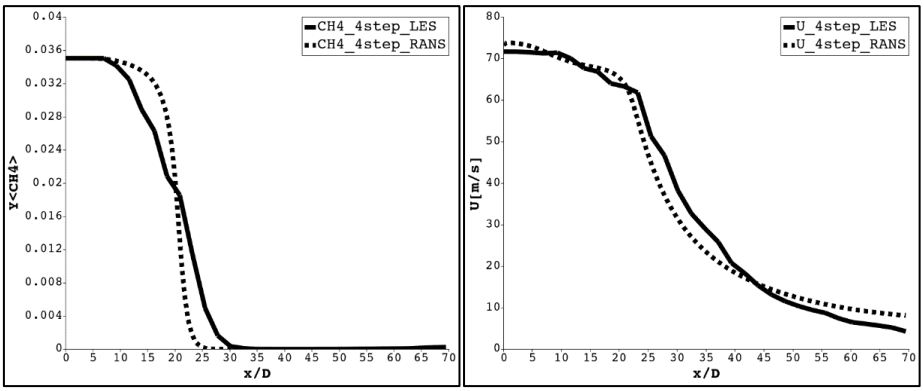

Figure 4.4: Mean CH_4 and velocity along the centerline of 5%CH_4+20%H_2 blending jet flame

4.4 RANS simulations of CH_4-H_2 blending jet flame with different proportions

4.4.1 CH_4-H_2 blending jet flame based on Sandia flame D

Four different blending fuel proportion jet flame RANS simulations have been considered: 20%CH_4+5%H_2, 15%CH_4+10%H_2, 10%CH_4+15%H_2, 5%CH_4+20%H_2. The case of pure 25% CH_4 is considered as a reference. The results of the mean mass fraction of CH_4, H_2, CO_2, O_2, temperature, and velocity along the centerline of flame are shown in figure 4.5. It can be observed that with the reduction of inlet CH_4, the emission of CO_2 also shows a corresponding downward trend. Besides, the consumption of O_2 also gradually decreases because there is still 3%O_2 remaining in the case with 5%CH_4+20%H_2, while it is completely consumed in the benchmark case.

The increase of hydrogen and decrease of methane in the main jet lead to an earlier peak temperature occurring, and the temperature decays faster after that. However, the temperature maintains the peak value consistent even though there are small fluctuations. Due to the constant Reynolds number condition, the inlet velocity of the main jet is revised according to the corresponding blending proportion of fuel. Therefore, the predicted velocities are raised at the exit of the main jet nozzle. Before reaching the peak temperature, the flame velocity decreases slowly, but it decays more rapidly after passing the position of peak temperature. The velocity drops to the same level, around 10m/s.

In addition, the conversion of fuel compositions has no noticeable effects on the velocity of the flame extremity. Hence, it can be concluded that the addition of hydrogen in the methane fuel accelerates the propagation and attenuation of the jet flame. But it allows the flame to keep the peak temperature and reduce the emission of CO_2 and consumption of O_2.

4.4.2 Pure 25%H_2 jet flame based on Sandia flame D

After the simulation of 5%CH_4+20%H_2 blending fuel jet flame, the following consideration is a complete replacement of CH_4 by H_2 in the main jet. Figure 4.6 shows the mean mass fraction of H_2, temperature, and velocity along the centerline of flame with three different chemical mechanisms. The Keromnes' mechanism is a hydrogen-air combustion mechanism proposed

by Keromnes et al.[20]. Simulation results between the 4-step and the Keromnes' mechanisms are quite similar, while they are apparently different from results with GRI-Mech 3.0, especially in the predicted temperature results. However, there are no experimental data for comparison. Then, a different hydrogen-air jet flame is used in the next chapter for validation.

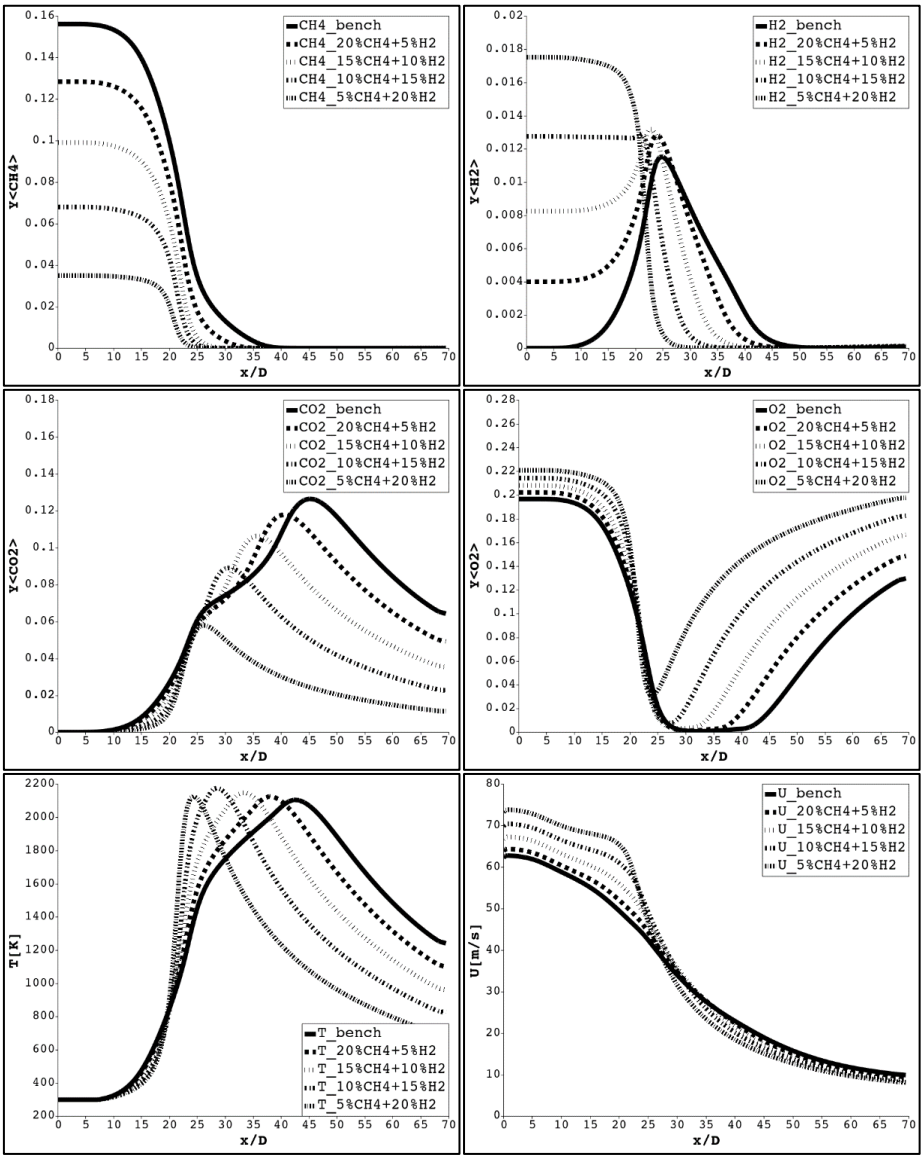

Figure 4.5: Mean CH_4, H_2, CO_2, O_2, temperature, and velocity along the centerline of CH_4-H_2 blending jet flame

4.4.3 H_2-air jet flame based on Barlow and Carter

To study the influence of chemical mechanisms on simulation of pure H_2-air jet flame, the flame reported by Barlow and Carter[15] in 1994 was selected. The flame shows two pre-inlet jets, including a hydrogen fuel jet at 296m/s and an air jet at 1m/s. The inner diameter of the fuel jet is 3.75 mm. The Reynolds number is 10000. Figure 4.7 shows the mean mass fraction of H_2, temperature, and velocity along the centerline of flame compared with experimental data.

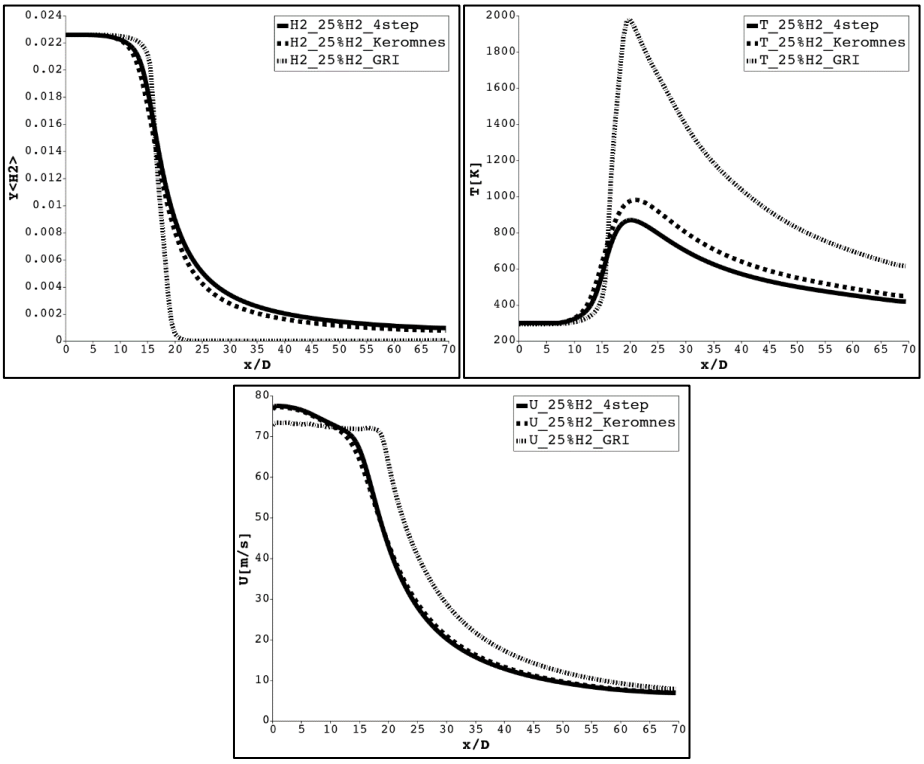

Figure 4.6: Mean H_2, temperature and velocity along the centerline of 25%H_2 jet flame

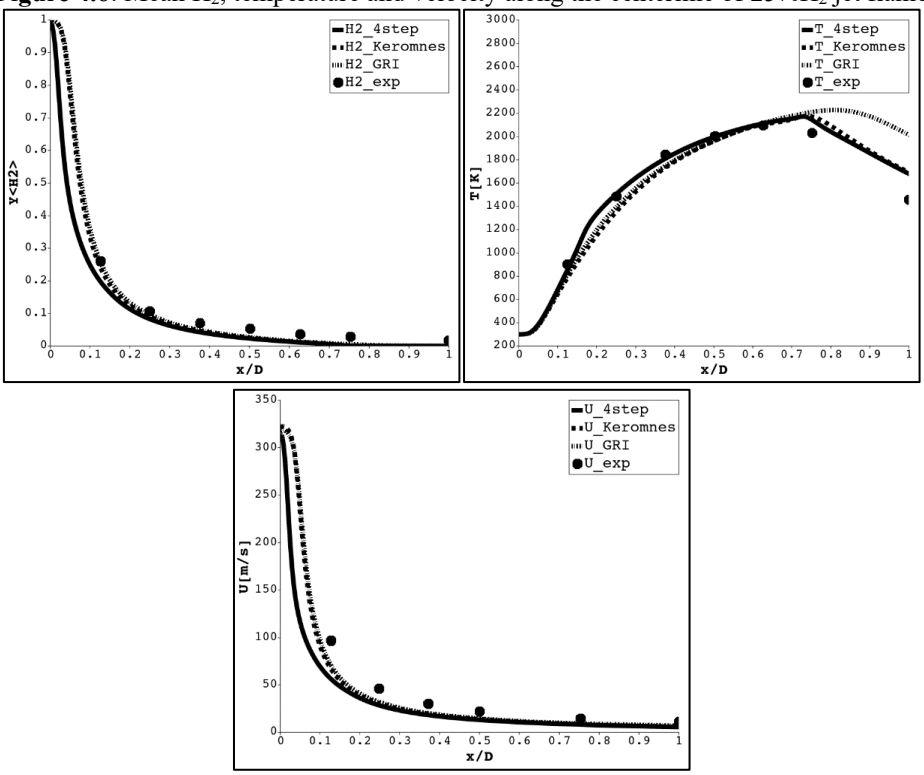

Figure 4.7: Mean H_2, temperature and velocity along the centerline of H_2-air jet flame by Barlow and Carter; experimental data from [15]

It can be observed that the predicted temperature with the 4-step and the Keromnes' mechanisms collapses well with the measured data, while the results with GRI-Mech 3.0 differs from the other curves. These results show the same trend as previous 25%H_2 fuel jet flame simulations. Hence, it means that the 4-step mechanism developed by Jones and Lindstedt can be regarded as a global mechanism when it is applied in pure hydrogen-air jet flame simulation.

5 CONCLUSIONS

A series of pure methane, methane-hydrogen blending, and pure hydrogen fuel jet flame simulations are conducted using Open FOAM. The primary purpose is focused on the effect of hydrogen addition to methane-air jet flame. The flame simulations consider different chemistry kinetic mechanisms, including the 1-step, 2-step, 4-step, DRM19, and GRI-Mech3.0. Two turbulence models, RANS/ $k-\varepsilon$ and LES/WALE, have been tested. Experimental data from Sandia flame D and hydrogen-air jet flame by Barlow and Carter are used for result validations. There are several conclusions obtained from this study:

- The 4-step mechanism gives good agreements with experimental data using both RANS and LES simulations of Sandia flame D. Other reduced and detailed mechanisms are not attractive because the accuracy and/or computational cost are insufficient.
- The addition of hydrogen to methane fuel would lead to a trend of earlier occurring temperature peak, and then temperature also drops faster. The flame velocity decays slowly before reaching the peak temperature, but it finally drops to the same level.
- On the other hand, the addition of hydrogen accelerates the heating and propagation of flame under the condition of a constant Re number in the main jet. It allows the flame to maintain the same peak temperature while reducing carbon dioxide emission and oxygen consumption.
- The pure hydrogen-air jet flame by Barlow and Carter is simulated with different chemical mechanisms, and results are validated by experimental data. The 4-step mechanism can be regarded as a global mechanism when it is applied in hydrogen-air jet flame simulation.

6 ACKNOWLEDGEMENTS

The author J. Liu has a scholarship from China Scholarship Council to complete PhD at the Technical University of Catalonia (UPC).

REFERENCES

[1] Bell, S.R. and Gupta, M. Extension of the lean operating limit for natural gas fueling of a spark ignited engine using hydrogen blending. *Combust. Sci. Technol* (1997) 123: 23–48.

[2] Sierens, R. and Rosseel, E. Variable composition hydrogen/natural gas mixtures for increased engine efficiency and decreased emissions. *J. Eng. Gas Turbines Power* (2000) 122: 135–140.

[3] Huang, J., Bushe, W.K., Hill, P.G., and Munshi, S.R. Experimental and kinetic study of shock initiated ignition in homogeneous methane-hydrogen-air mixtures at engine-relevant conditions. *Int. J. Chem. Kinet* (2006) 38: 221–233.

[4] Huang, Z., Lu, L., Jiang, D., Xing, D., and Ren, Z.J. Electrochemical hythane production

for renewable energy storage and biogas upgrading. *Appl. Energy* (2017) 187: 595–600.
[5] Fordoei, E.E., Mazaheri, K., and Mohammadpour, A. Effects of hydrogen addition to methane on the thermal and ignition delay characteristics of fuel-air, oxygen-enriched and oxy-fuel MILD combustion. *Int. J. Hydrogen Energy* (2021) 46: 34002–34017.
[6] Karbasi, M. and Wierzba, I. The effects of hydrogen addition on the stability limits of methane jet diffusion flames. *Int. J. Hydrogen Energy* (1998) 23: 123–129.
[7] Deniz, Y. and Seyhan, U.O. Computational modeling of hydrogen enriched non-premixed turbulent methane air flames. *Proc. Eur. Combust. Meet* (2005) 1–6.
[8] Mardani, A. and Tabejamaat, S. Effect of hydrogen on hydrogen-methane turbulent non-premixed flame under MILD condition. *Int. J. Hydrogen Energy* (2010) 35: 11324–11331.
[9] Barlow, R.S., Frank, J.H., Karpetis, A.N., and Chen, J.Y. Piloted methane/air jet flames: Transport effects and aspects of scalar structure. *Combust. Flame* (2005) 143: 433–449.
[10] Christ, D. Simulating the combustion of gaseous fuels. *6th OpenFoam Workshop Training Session* (2011) 13–16.
[11] Franzelli, B., Riber, E., Gicquel, L.Y.M., and Poinsot, T. Large Eddy Simulation of combustion instabilities in a lean partially premixed swirled flame. *Combust. Flame* (2012) 159: 621–637.
[12] Jones, W.P. and Lindstedt, R.P. Global reaction schemes for hydrocarbon combustion. *Combust. Flame* (1988) 73: 233–249.
[13] Kazakov, A. and Frenklach, M. Reduced reaction sets based on GRI-Mech 1.2. (1994) http//www. me. berkeley. edu/drm.
[14] Smith, G.P. GRI-Mech 3.0 (1999) http//www. me. berkley. edu/gri_mech/.
[15] Barlow, R.S. and Carter, C.D. Raman/Rayleigh/LIF measurements of nitric oxide formation in turbulent hydrogen jet flames. *Combust. Flame* (1994) 97: 261–280.
[16] Mousavi, S.M. Combination of reactingFoam and chtMultiRegionFoam as a first step toward creating a multiRegionReactingFoam, suitable for solid/gas phase. *Proceedings of CFD with OpenSource Software* (2019).
[17] Jones, W.P., Launder, B.E. The prediction of laminarization with a two-equation model of turbulence. *Int. J. Heat Mass Transf* (1972) 15: 301–314.
[18] Nicoud, F., Ducros, F. Subgrid-scale stress modelling based on the square of the velocity gradient tensor. *Flow, Turbul. Combust* (1999) 62: 183–200.
[19] Magnussen, B.F. The Eddy Dissipation Concept---A Bridge Between Science and Technology. *ECCOMAS Themat. Conf. Comput. Combust* (2005).
[20] Kéromnès, A., Metcalfe, W.K., Heufer, K.A., et al. An experimental and detailed chemical kinetic modeling study of hydrogen and syngas mixture oxidation at elevated pressures. *Combust. Flame* (2013) 160: 995–1011.